What will the next generation radio telescope detect at 1.4 GHz?

A. Hopkins[1]
Australia Telescope National Facility, PO Box 76 Epping, NSW 1710, Australia.
and

R. Windhorst
Dept. of Physics & Astronomy, Arizona State University, Box 871504, Tempe, AZ 85287-1504, USA
and

L. Cram
Astrophysics Department, School of Physics, University of Sydney, NSW 2006, Australia
and

R. Ekers
Australia Telescope National Facility, PO Box 76 Epping, NSW 1710, Australia.

ABSTRACT

An international project is underway to design and build a radio telescope with an effective collecting area two orders of magnitude greater than the largest existing instruments. One of the many scientific goals of this instrument will be the investigation of the extragalactic radio source population at flux densities two to three orders of magnitude fainter than the limits of existing observations. We present simulations of the radio sky at 1.4 GHz down to such flux density limits using known radio luminosity functions and their extrapolations for two different population scenarios. The resulting simulations will assist design studies for the new telescope.

Subject headings: galaxies: evolution — galaxies: general — galaxies: luminosity function

[1] School of Physics, University of Sydney, NSW 2006, Australia.

1. Introduction

The next generation radio telescope will be used to address a number of key scientific questions, including establishing the redshift of reionisation (Shaver et al. 1999), detection of the precursors of the first galaxies through HI, measuring the mass function of black holes in galaxy cores, pulsar detection and timing in other galaxies as well as our own, and investigation of star-formation processes and radio emission from stars, among many others no less inspiring (Braun & Taylor 1999, Hopkins et al. 1999c). In addition there will be unanticipated discoveries which may represent the most significant results from the instrument. However, since we cannot predict the nature of serendipitous discoveries, we are limited to identified goals. This paper investigates the implications of our current knowledge about extragalactic radio source populations on the results of anticipated 1.4 GHz radio continuum observations with such an instrument.

A number of published radio surveys probe the population of microjansky ($< 10\,\mu$Jy) radio sources (Windhorst et al. 1993a, Windhorst et al. 1995, Richards et al. 1998, Hopkins et al. 1998, Hopkins et al. 1999b, Norris et al. 1999). Below a few mJy, the 1.4 GHz population begins to be dominated by starburst and disk galaxies, whose radio emission derives primarily from star formation processes (Windhorst et al. 1985, Kron et al. 1985, Benn et al. 1993, Fomalont et al. 1997, Georgakakis et al. 1999), as opposed to the classical radio sources fuelled by active galactic nuclei (AGN), which dominate at higher flux densities. Interest in the sub-millijansky population stems from the desire to investigate the nature of star-formation in galaxies, particularly at large redshift. This population has the potential, through radio-selection, to provide very large, homogeneously selected samples of actively star-forming galaxies over a wide range in redshift. Current surveys are only just starting to compile such large samples, approaching thousands of objects (Georgakakis et al. 1999, Hopkins et al. 1999b). With the anticipated sensitivity at nJy levels, resolution of $0\farcs1$ and field size of one square degree at 1.4 GHz, surveys with the next generation radio telescope will rapidly dwarf present surveys.

To investigate the implications of current models describing the 1.4 GHz radio population, we have begun a program of simulating aspects of the radio sky at this wavelength. Throughout this paper we use $H_0 = 50\,\mathrm{km\,s^{-1}\,Mpc^{-1}}$ and $q_0 = 0.5$.

2. The model

The local 1.4 GHz luminosity function (LF) is quite well determined down to $L \approx 10^{18.5}\,\mathrm{WHz^{-1}}$ (Condon 1989). LFs invoking luminosity evolution models for the AGN population (Dunlop & Peacock 1990) and the starburst population (Rowan-Robinson et al. 1993, Hopkins et al. 1998) match the observed 1.4 GHz source counts down to the flux density limits of current observation. The model presented here extrapolates the 1.4 GHz luminosity functions for several radio source populations to luminosities much fainter than have been observed. This is supplemented by distributions in linear size of the objects, effectively to provide a "model universe," which is then projected onto the desired two-dimensional field of view. Although the effects of large scale structure have been ignored in this initial model, they will be included as the work is refined, adding the ability to test various clustering models against observation. The model also allows the simulation of different cosmologies, and different rates and types of evolution for direct comparison to observation. In practice this requires the development of different luminosity function models and evolutionary rates for each cosmology of interest, to ensure the source counts predicted from the model are consistent with existing observations.

2.1. Radio source populations

Earlier work on modelling 1.4 GHz radio luminosity functions has been successful in establishing models which accurately reproduce the observed source counts after invoking luminosity evolution (Dunlop & Peacock 1990, Rowan-Robinson et al. 1993). These models have been adopted for the current investigation. The galaxy populations used for our simulations comprise four distinct types of radio sources which we broadly classify as "AGN" or "starforming" according to whether the radio emission for the population is derived predominantly from a central engine or from star-formation processes, respectively. We have divided the AGN class into steep-spectrum and flat-spectrum radio sources, following Dunlop & Peacock (1990). The luminosity functions corresponding to these two populations have the form (Dunlop &

Peacock 1990):

$$\phi = \phi_0 \left\{ \left(\frac{L_{1.4}}{L_c(z)} \right)^{\alpha} + \left(\frac{L_{1.4}}{L_c(z)} \right)^{\beta} \right\}^{-1}, \qquad (1)$$

with parameters

$$\begin{aligned} \phi_0 &= 10^{-6.91}, \\ \alpha &= 0.69, \\ \beta &= 2.17, \\ L_c(z) &= 26.22 + 1.26z - 0.26z^2, \end{aligned}$$

for steep spectrum AGN, and

$$\begin{aligned} \phi_0 &= 10^{-8.15}, \\ \alpha &= 0.83, \\ \beta &= 1.96, \\ L_c(z) &= 26.36 + 1.18z - 0.28z^2, \end{aligned}$$

for flat spectrum AGN. The luminosity evolution of this population is included in the redshift dependence of $L_c(z)$. This evolution results in a redshift cutoff in the population beyond $z \approx 2$ (Dunlop & Peacock 1990), which can be seen in the redshift distributions from the simulations (Section 3).

The starforming class includes what we refer to as "IRAS-type" galaxies, for which we have used the $60\,\mu$m "warm IRAS" galaxy luminosity function of Saunders et al. (1990), after conversion to 1.4 GHz assuming $L_{60} = 100 L_{1.4}$ (Rowan-Robinson et al. 1993). This IRAS-type population is identified with the "starburst" galaxy population which begins to dominate the 1.4 GHz source counts below a few millijanskies. Their luminosity function has the form (Saunders et al. 1990, Rowan-Robinson et al. 1993):

$$\phi(L) = C \left(\frac{L}{L^*} \right)^{1-\alpha} \exp \left[-\frac{1}{2\sigma^2} \log_{10}^2 \left(1 + \frac{L}{L^*} \right) \right], \qquad (2)$$

with parameters (assumed the same at $60\,\mu$m and 1.4 GHz) of $\alpha = 1.27$, $\sigma = 0.626$, and $C = 3.25 \times 10^{-2}$. At $60\,\mu$m, $L^*_{60} = 10^{23.9}\,\mathrm{WHz}^{-1}$ so from the radio/FIR correlation, $L^*_{1.4} = 10^{21.9}\,\mathrm{WHz}^{-1}$. The luminosity evolution for this population is of the form $L(z) \propto (1+z)^Q$ with $Q = 3.3$. A form of redshift cutoff at $z = 2$ was used in this evolution, also. For $z > 2$ the evolution was calculated as though the source was at $z = 2$, i.e. $L(z) \propto (1+2)^Q$ (Hopkins et al. 1998).

Radio emission can be produced through star-formation processes, and can be interpreted as an indicator of the current star-formation rate (SFR) in a galaxy if no AGN emission is present (Cram et al. 1998). Hence, as observational sensitivity improves, the so-called "normal" galaxies will eventually be detectable through their radio emission even though their SFRs may be quite low. The resulting population of "normal" galaxies detected through radio emission may be adequately represented by the faint end tail of the "warm IRAS" luminosity function, and we have constructed several simulations under this assumption. Alternatively, there is the possibility that an additional luminosity function needs to be invoked to account for galaxies with only modest levels of star formation. Certainly the radio source counts derived from the "warm IRAS" luminosity function lie well below the maximum upper limit derived from limits on the cosmic background radiation (CBR) fluctuations (Fomalont et al. 1993, Windhorst et al. 1993b, Windhorst 1999).

To derive a luminosity function for the modest starformers, allowing them to be included in our simulations, we have chosen to make use of the known luminosity function for optical galaxies, the great majority of which have low SFRs. Accurately modelling the radio properties for such a population from the known optical luminosity function, however, requires a knowledge of the bivariate (radio-optical) luminosity function (BLF) over a large range of luminosities. Despite the limits to the current knowledge of the BLF (Auriemma et al. 1977, Sadler et al. 1989, Hopkins et al. 1999b), an attempt to include this population was made, using an over-simplified model. An optical (B_J-band) luminosity function (a schechter function with parameters (Efstathiou et al. 1988) $\alpha = -1.1$, $\phi^* = 0.0156$ and $M^* = -19.9$ mag, which corresponds to $L^* = 10^{21.5}\,\mathrm{WHz}^{-1}$ at 440 nm), was used. This was converted to a radio luminosity function using the simple assumption of a constant radio/optical luminosity ratio. One possibility for refining this assumption could be to use a luminosity ratio distribution closer to the observed distribution in the far-infrared/optical luminosity ratio (Corbelli et al. 1991, Rowan-Robinson et al. 1987), by invoking the radio/FIR correlation, although we have not explored this extra parameter space in the current investigation. The ratio chosen was $L_{1.4}/L_{opt} = \frac{1}{3}$ (for $L_{1.4}$ and L_{opt} in units of WHz^{-1}), which corresponds to a SFR of $\approx 0.26\,M_\odot\mathrm{yr}^{-1}$ for an optical L^* galaxy (from equation 1 of Cram et al. 1998). This ratio is the highest possible (constant) value consistent with the observed counts and the contributions from the other populations. The resulting luminosity function, combined with the other populations, has been used to predict the source counts to a flux density of 1 nJy (Figure 1). The symbols in this Figure come from two main sources, the crosses are a compilation of 1.4 GHz source counts from Windhorst et al. (1993a), and the circles from the *Phoenix Deep Survey* (Hopkins et al. 1999b, and references therein). The thick dashed line shown in this and succeeding Figures is the upper limit to the source counts derived from known limits to the CBR fluctuations (Fomalont et al. 1993, Windhorst et al. 1993b, Windhorst 1999). If the source count continues toward fainter flux densities from the limits of existing observations with the constant slope seen between about 0.05–1 mJy ($\gamma = 2.3$, where the differential source counts $n(S) \propto S^{-\gamma}$), then the count must ultimately converge below about 100 nJy (± 0.5 dex) with a slope $\gamma \leq 2$.

It is possible that there could be a greater contribution from the normal galaxy population if the rate of luminosity evolution invoked for the IRAS-type galaxies were lower. Such a scenario is reflected in the source counts shown in Figure 2. In this Figure we show source counts predicted under the assumption that the IRAS-type galaxies undergo luminosity evolution at a rate $L(z) \propto (1+z)^Q$ with $Q = 2.8$ rather than the $Q = 3.3$ rate used in Figure 1. The luminosity ratio used for the normal galaxies in Figure 2 is $L_{1.4}/L_{opt} = 0.8$ (corresponding to a SFR of $\approx 0.63\, M_\odot \mathrm{yr}^{-1}$ for an optical L^* galaxy). Uncertainty in the $60\,\mu$m luminosity function normalisation leads to an uncertainty in the magnitude of the predicted source counts. This is indicated by the vertical error bar shown on the counts for the IRAS-type galaxies. Any additional population should not increase the contribution of the starforming galaxies outside this range. Hence, it is worth remembering that there are several free parameters in this analysis, although we have restricted this investigation to predictions from only two scenarios. These scenarios both include the two components of the AGN population, combined with a starforming population being comprised of 1) IRAS-type galaxies only, and 2) IRAS-type galaxies plus normal galaxies with $L_{1.4}/L_{opt} = \frac{1}{3}$.

2.2. Linear source sizes

The distribution in linear size of radio sources at 1.4 GHz has been studied extensively for the population we are referring to as AGN. Indeed, the variation in angular sizes of radio sources with redshift is a classic test for investigating cosmological models (Hooley et al. 1978, for example). In more recent work describing the variation of linear size with redshift (Gopal-Krishna 1991, Kapahi 1989, Onuora 1989, Singal 1988, Oort et al. 1987, Allington-Smith 1984, for example) the general consensus is that for $z \lesssim 1.5$ the linear size of these (steep-spectrum) radio sources evolves as

$$l = \frac{l_0}{(1+z)^3} P^{0.3}, \tag{3}$$

(see also Subramanian & Swarup 1990). Here l is the proper length of the galaxy. This relation reflects the evolution of the characteristic length (l_0) of the steep-spectrum AGN population, combined with the distribution (dependent on P) of individual source sizes within that population. A value of $l_0 = 3 \times 10^{-6}\,\mathrm{kpc}\,(\mathrm{WHz}^{-1})^{-0.3}$ was used for consistency with Subramanian & Swarup (1990). In our simulations we have adopted this relationship for $z < 1.5$. For larger redshifts, $z = 1.5$ was used when calculating the intrinsic linear size of a source (i.e. $l = l_0/(1+1.5)^3 P^{0.3}$). The angular size for all sources is derived from the intrinsic linear size, l, in Mpc, calculated as just described, and the actual redshift, z, by

$$\theta = l \frac{(1+z)^2}{d_L}, \tag{4}$$

where d_L is the luminosity distance

$$d_L = \frac{c}{H_0 q_0^2}(q_0 z + (q_0 - 1)(\sqrt{1 + 2q_0 z} - 1)). \tag{5}$$

Some recent work (Blundell et al. 1999) suggests that the above parametrisation of linear size is too simplistic and is biased by catalogue specific selection effects, and that the true distributions are much more complex. This should be kept in mind when our simulations are presented.

There is evidence that in galaxies with higher levels of star-formation activity, this activity is concentrated in smaller regions than for less active galaxies (van Driel et al. 1991). For the more modest starforming galaxies the extent of the radio emission (coming predominantly from supernovae and HII regions) is likely to be larger, but primarily restricted to the size of the optical disk. For the IRAS-type population a distribution of 1.4 GHz linear sizes was derived from the radio sizes of IRAS galaxies (van Driel et al. 1991, Eales et al. 1988), and a distribution of half-light radii for disk galaxies (Roche et al. 1998) was used for the normal galaxy population. These distributions are both luminosity dependent. The relation for IRAS-types was drawn from Figure 4 of van Driel et al. (1991) and converted to 1.4 GHz using a spectral index of -0.7 giving:

$$\log(l) = 0.5\log(L_{1.4}) - 10.8 \tag{6}$$

where l is the linear size in kpc and $L_{1.4}$ the luminosity in WHz^{-1}. This relation was also used for the flat-spectrum AGN population, which is typically composed of quite compact sources. The relation for the normal galaxies is

$$\log(r_{\mathrm{hl}_0}) = -0.2M_B - 3.30 \tag{7}$$

and using evolution of the half-light radius, r_{hl_0}, of the form $r_{\mathrm{hl}} = (1-0.2z)r_{\mathrm{hl}_0}$ approximated from Figure 2 of Roche et al. (1998). This evolution was truncated at $z = 4$ so that beyond this limit r_{hl} was calculated as though the source was at $z = 4$. These parametrisations are intended to be representative rather than exhaustive, as obviously galaxies of the same luminosity can have quite different physical sizes. The values determined for the IRAS-type galaxies are typically an order of magnitude smaller than those for the normal population, consistent with the result found by Eales et al. (1988) that radio sizes of high FIR luminosity IRAS sources are about a tenth the size of the optical galaxy. This is also consistent with the result that in disk galaxies the scale-length of the disk is about ten times the effective radius of the bulge (de Jong 1996, Figure 18, particularly K-band results which are less likely to be affected by extinction).

The resulting simulations (see below) turn out to be quite sensitive to the distributions chosen here, as the numbers of starforming galaxies are very large when faint flux density limits are chosen. Accordingly, this aspect of the simulation would benefit from a more accurate parametrisation of the linear sizes of faint optical galaxies as a function of luminosity and redshift.

2.3. Simulated Images

Simulated images from the information contained in the models are constructed as follows. The luminosity functions and evolutionary models are used to define the number, luminosity and redshift of sources in a specified field of view, above a given flux density limit. The luminosities are combined with redshifts and the chosen cosmology to produce flux densities for each source. Similarly, the intrinsic sizes are used to derive apparent angular sizes for each source. Each source is indicated in the image by a two-dimensional gaussian distribution of the total flux density, with random position angle. The apparent ellipticity distribution of faint field galaxies changes very little from $B = 15$ to $B = 27$ mag (Odewahn et al. 1997), so in a sense the distribution of ellipticities is intrinsically random and hardly affected by evolutionary effects, even though the galaxy morphology changes noticeably between $B = 15$ and $B = 27$. To model the observed axial ratio, R, of the gaussian for disk systems we refer to the results of Lambas, Maddox & Loveday (1992) who find that a pure oblate model for disk galaxies fails to reproduce the observed axial ratios. However, a nearly oblate model with intrinsic axial ratio $r = 0.2$ can produce consistent fits to the observations. Binney & de Vaucouleurs (1981) also find a range $0.15 < r < 0.35$ derived for spiral galaxies from the Second Reference Catalogue of Bright Galaxies (de Vaucouleurs, de Vaucouleurs & Corwin 1976), and state that later type spirals have distributions which peak at smaller values of r. For simplicity, then, we have assumed each disk is an oblate ellipsoid with intrinsic axial ratio of $r = 0.2$. A random angle of inclination, i, is chosen which then gives the observed axial ratio, R, as

$$R = \sqrt{r^2 + (1-r^2)\cos^2 i}. \tag{8}$$

The source so constructed is randomly positioned within the specified field of view, and coloured according to type, red for AGNs and blue for starformers. If sources overlap, their flux densities are simply added together, producing appropriate colour combinations if they are not the same colour source. No attempt to include the effects of obscuration or gravitational lensing has been made, although these could in principle be added to the model.

In addition, as an elementary step toward modelling the double-lobed nature of many real AGNs, a pair of adjacent elliptical gaussians have been used for the steep spectrum sources, rather than the single elliptical gaussian used for flat spectrum AGNs and starformers. This is an unrealistic over-simplification, particularly as no orientation effects, beaming, or more complicated morphologies have been contemplated. The usefulness of refinements to this aspect of the display can be debated, but for the current purpose this simple step was deemed sufficient.

3. Simulations

The algorithm described above has been used to create simulated radio images for a wide variety of field sizes and flux density limits. Many simulations were investigated but here we present only two, indicative of our results, for analysis in terms of the properties of the next generation radio telescope.

The first example is shown in Figure 3, a simulation with a field size of $5' \times 5'$, about four times the size of the Hubble Deep Field (HDF) (Richards et al. 1998, for example). For this simulation the starformers are represented by the IRAS-type population only. A flux density limit of $0.1\,\mu$Jy has been used and over 1000 sources brighter than this limit are predicted (a source density of $\sim 4.8 \times 10^8\,\mathrm{sr}^{-1}$).

Consistency checks have been performed to confirm that the simulated distributions in flux density agree with the models used to produce them. Source counts for the simulation in Figure 3 are shown in Figure 4 along with the (continuous) source counts derived from the assumed luminosity functions and evolution. Typical luminosity and redshift distributions have been derived from the simulations and are presented in Figure 5.

A second simulation of a $5' \times 5'$ region is shown in Figure 6, again with a flux density limit of $0.1\,\mu$Jy, this time including the population of normal galaxies. A total of 1941 sources (574 AGN, 1367 starformers) are predicted, giving a source density of $\sim 9.2 \times 10^8\,\mathrm{sr}^{-1}$. Again, source counts, luminosity and redshift distributions are shown (Figures 7 and 8). It can be seen that even with this scenario and at these faint levels, while the starformer population is dominant the AGN population is certainly not negligible. A hint of this effect may be seen in recent work in the optical domain (Sarajedini et al. 1999) showing that $\approx 10\%$ of HST Medium Deep Survey galaxies (to $z \approx 0.8$) may be low luminosity AGNs (implied through the presence of unresolved nuclear components which contribute noticeably to the total galaxy light). There is also a very clear distinction between the two scenarios (starformers comprised of IRAS-types only compared to the inclusion of a normal galaxy population) in terms of the number of sources predicted. This is a prediction which will easily distinguish between the scenarios when next generation radio telescope observations are eventually made.

The absence of very large and bright AGN type sources in the simulated fields shown is a result of presenting simulated fields coincidentally free of such objects. This mimics the careful selection against bright sources typical in deep radio surveys, as well as ensuring clarity in the displayed simulations. Typically a simulated field of this size may contain one or two sources of several tens of millijanskies, and with physical sizes dominating the field.

The limiting flux density value of $0.1\,\mu$Jy was chosen since that is the expected 5σ level for an interferometer having the specifications given for the next generation radio telescope after an integration of 12 hours. The relevant specifications are an effective area to system temperature ratio of $A_{\mathrm{eff}}/T_{\mathrm{sys}} = 2\times10^4\,\mathrm{m}^2\mathrm{K}^{-1}$ with two simultaneous frequency bands and a bandwidth $\Delta\nu = 500\,\mathrm{MHz}$ at $1.4\,\mathrm{GHz}$. Deeper images will obviously be attainable with longer integrations. For example, the time spent observing the HDF with the Very Large Array (Richards et al. 1998) was 152 hours of integration. Some recent observations of similar integration time with the Australia Telescope Compact Array are provided by Hopkins et al. (1999b) and Norris et al. (1999). With this integration time the next generation radio telescope would reach a 5σ detection level of about 30 nJy!

4. Discussion

There is a notable feature in the luminosity distributions for all the simulations: IRAS-type galaxies, rather than AGN, actually dominate at the brightest luminosity end (see Figures 5 and 8). In fact, in each simulation the brightest source is an AGN object, but between luminosities of about $10^{22}\,\mathrm{WHz}^{-1}$ and $10^{24.5}\,\mathrm{WHz}^{-1}$ the IRAS-types dominate. This result can be explained as a combination of the small area being sampled, and the dearth of AGN-type galaxies further than $z \approx 3$. This redshift cutoff in the distribution of AGN sources results from the chosen model of luminosity evolution for this population (Dunlop & Peacock 1990).

The redshift distribution for the "normal" galaxies (Figure 8) shows no objects further than redshifts of $z \approx 2$ in these simulations. This is not a feature of the models used as for the AGN population, but is instead dependent on the flux density limits chosen for the simulation. Had the limits been fainter, such objects (having only modest intrinsic luminosities, predominantly $< 10^{22}\,\mathrm{WHz}^{-1}$, as can be seen from the luminosity distribution in Figure 8) would have been detected at continually higher redshifts. Additionally, the distribution of luminosities for this population is very narrow, concentrated primarily within two orders of magnitude. This is a reflection of the shape of the optical luminosity function from which this population is derived, and it is useful to emphasise the very small range of intrinsic luminosities displayed by galaxies at optical wavelengths compared to the range of ten orders of magnitude or more possible in a galaxy's intrinsic radio luminosity.

The limited overlapping of objects in the simulated images implies that the natural confusion level has not yet been reached for the majority of sources, and only the largest and brightest are likely to be affected. If the instrumental resolution (synthesised beam FWHM) is set at $0\farcs1$, there are 9×10^6 beams within a field the size of the simulations presented. This allows for 90000 sources if 100 beams are required per source to avoid the effects of instrumental confusion. This will not be a problem with only the few thousand sources predicted over this field size. Even with a synthesised beam size of $0\farcs6$ instrumental confusion at this flux density level would only barely be a problem with this many sources. With a flux density limit of 20 nJy and the same $5' \times 5'$ field of view, our current simulations predict only 6000 sources, (requiring a resolution of $\lesssim 0\farcs38$ to avoid instrumental confusion), although the possibility of further new populations contributing to the source counts should not be ignored. Obviously, though, the possibility of much longer integrations to probe even fainter populations, along with the desire to make detailed images of the larger, resolved sources would require a higher resolution. This is also desirable for obtaining reliable optical galaxy counterparts to the radio sources detected.

The extent of the natural confusion is directly related to the intrinsic distribution of linear sizes for the starforming population (as opposed to the models used in these simulations). If the true distribution is dominated by objects with quite small half-light radii (only a few kpc, c.f. Odewahn et al. 1996) the effects of natural confusion, to the level of the $0.1\,\mu$Jy investigated here, will be mild. At the anticipated high resolution many of the sources will be resolved, and the design of a telescope wishing to image such fields at these faint flux densities will require its high sensitivity response over baselines corresponding to this high resolution. This implies that a significant fraction of the collecting area needs to be distributed over long baselines (up to hundreds of kilometres for operation at 1.4 GHz). Obviously there is a trade-off between resolution and surface brightness sensitivity, and an optimum solution needs to be established. Another effect arising from the choice of telescope configuration is the intensity and distribution of the sidelobe response of the instrument. This is also of importance, since to detect a $0.1\,\mu$Jy source in the vicinity of very bright sources (flux densities up to hundreds of millijanskies) requires a very high dynamic range in the image, up to 10^6 after deconvolution. Obviously very deep radio surveys will continue to be carried out in carefully selected regions, chosen to be free of such bright sources. However, the field of view of the next generation radio telescope has been specified to be one square degree at 1.4 GHz, and in all but a few regions of this size there are likely to be sources of at least several tens of millijanskies. It appears that very deep radio surveys with the next generation radio telescope are much more likely to be dynamic range limited than confusion limited. Clearly, the better the dynamic range in the synthesised beam the easier it will be to achieve the required high dynamic ranges in resulting images, although there are many other contributing factors which also need to be considered.

The large field of view specified for this instrument is 144 times the area of the simulations presented here, hence observations down to $0.1\,\mu$Jy will result in something of the order of 3×10^5 sources per field. This has implications for the nature and sophistication of automated source detection and characterisation algorithms which must be developed to analyse such data. Also, since a well sampled image will have several pixels across a synthesised beam FWHM (specified to be $0\farcs1$), an image of a one square degree field will be of the order of $10^5 \times 10^5$ pixels in size. Although the tens of gigabytes per image required for storage will not be a problem, visual inspection of entire images at full resolution will become difficult in the extreme, and will likely be reserved for objects denoted as interesting by automated classifiers.

5. Conclusions

We have initiated a program of simulations of the 1.4 GHz sky to investigate the implications of existing models for luminosity functions, luminosity evolution and linear size distributions on anticipated observations by the next generation radio telescope. The results are self-consistent and consistent with observed source counts, although there are still free parameters. Many simulations have been investigated and a limited selection of them presented here. The simulations produced with a flux density limit of $0.1\,\mu$Jy show fields which are dominated by starforming galaxies, although the proportion of AGN galaxies is still significant, even at such faint flux densities. The level of natural confusion in these fields is very strongly related to the choice of models for intrinsic linear size of the starformers, and deserves closer attention. To model different rates of evolution and different cosmologies, additional luminosity function models are necessary which correctly reproduce the observed source counts in each of the chosen scenarios.

The preliminary specifications for the next generation radio telescope (Braun & Taylor 1999) have been discussed in the context of the simulations presented here. There would appear to be only minor problems due to natural confusion at the levels of $0.1\,\mu$Jy, and no problems with instrumental confusion given the specified resolution of $0\overset{\prime\prime}{.}1$ even at much lower flux densities. The large field of view combined with the high resolution will necessarily affect the way images are analysed, reducing the level of visual interpretation, but won't pose a computational problem.

AMH and LEC acknowledge financial support from the Australian Research Council and the Science Foundation for Physics within the University of Sydney. RAW acknowledges grant AST-9802963 from the National Science Foundation, and NASA grants GO-5985.01-94A and GO-6609.01-95A from STScI under NASA contract NAS5-26555. The Australia Telescope is funded by the Commonwealth of Australia for operation as a National Facility managed by CSIRO.

REFERENCES

Allington-Smith J. R., 1984, MNRAS, 210, 611

Auriemma C., Perola G. C., Ekers R. D., Fanti R., Lari C., Jaffe W. J., Ulrich M. H., 1977, A&A, 57, 41

Benn C. R., Rowan–Robinson M., McMahon R. G., Broadhurst T. J., Lawrence A., 1993, MNRAS, 263, 98

Binney J. & de Vaucouleurs G., 1981, MNRAS, 194, 679

Blundell K. M., Rawlings S., Willott C. J., 1999, AJ, 117, 677

Braun, R., Taylor, R., Eds., "Square Kilometre Array Radio Telescope – The Science Case" 1999 URSI Large Telescope Working Group

Condon J. J., 1989, ApJ, 338, 13

Corbelli E., Salpeter E., Dickey J., 1991, ApJ, 370, 49

Cram L., Hopkins A., Mobasher B., Rowan-Robinson M., 1998, ApJ, 507, 155

de Jong R. S., 1996, A&A, 313, 45

de Vaucouleurs G., de Vaucouleurs A. & Corwin, 1976, *Second Reference Catalogue of Bright Galaxies,* University of Texas Press, Austin

Dunlop J. S. & Peacock J. A., 1990, MNRAS, 247, 19

Eales S. A., Wynn-Williams C. G., Beichman C. A., 1988, ApJ, 328, 530

Efstathiou G., Ellis R. S., Peterson B. A., 1988, MNRAS, 232, 431

Fomalont E. B., Partridge R. B., Lowenthal J. D., Windhorst R. A., Partridge R. B., 1993, ApJ, 404, 8

Fomalont E. B., Kellermann K. I., Richards E. A., Windhorst R. A., Partridge R. B., 1997, ApJ, 475, L5

Georgakakis A., Mobasher B., Cram L., Hopkins A., Lidman C., Rowan-Robinson M., 1999, MNRAS, (in press)

Gopal-Krishna, 1991, A&A, 248, 415

Hooley A., Longair M. S., Riley J. M., 1978, MNRAS, 182, 127

Hopkins A. M., Mobasher B., Cram L., Rowan-Robinson M., 1998, MNRAS, 296, 839

Hopkins A. M., Cram L., Mobasher B., Georgakakis A., 1999a, in “Looking Deep in the Southern Sky,” eds R. Morganti & W.J. Couch, (Springer:Berlin), 120

Hopkins A., Afonso J., Cram L., Mobasher B., 1999b, ApJL, (accepted)

Hopkins A., Ekers R., Jackson C., Cram L., Green A,. Manchester R., Staveley-Smith L., Norris R., 1999c, PASA, (in press)

Kapahi J. A., 1989, AJ, 97, 1

Kron R. G., Koo D. C., Windhorst R. A., 1985, A&A, 146, 38

Norris R., Hopkins A., Sault R., Ekers R., Ekers J., Badia F., Higdon J., Wieringa M., Boyle B., Williams R., 1999, AJ, (in preparation)

Odewahn S. C., Windhorst R. A., Driver S. P., Keel W. C., 1996, ApJ, 472, L13

Odewahn S. C., Burstein D., Windhorst R. A., 1997, AJ, 114, 2219

Onuora L. I., 1989, Ap&SS, 162, 343

Oort M. J. A., Katgert P., Windhorst R. A., 1987, Nature, 328, 500

Richards E. A., Kellermann K. I., Fomalont E. B., Windhorst R. A., Partridge R. B., 1998, AJ, 116, 1039

Roche N., Ratnatunga K., Griffiths R. E., Im M., Naim A., 1998, MNRAS, 293, 157

Rowan-Robinson M., Benn C. R., Lawrence A., McMahon R. G., Broadhurst T. J., 1993, MNRAS, 263, 123

Rowan-Robinson M., Helou G., Walker D., 1987, MNRAS, 227, 589

Sadler E. M., Jenkins C. R., Kotanyi C. G., 1989, MNRAS, 240, 591

Sarajedini V. L., Green R. F., Griffiths R. E., Ratnatunga K., 1999, ApJ, 514, 746

Saunders W., Rowan-Robinson M., Lawrence A., Efstathiou G., Kaiser N., Ellis R. S., Frenk C. S., 1990, MNRAS, 242, 318

Shaver P. A., Windhorst R. A., Madau P., de Bruyn G. 1999, A&A, (in press, astro-ph/9901320)

Singal A. K., 1988, MNRAS, 233, 87

Subramanian K. & Swarup G., 1990, MNRAS, 247, 237

van Driel W., van den Broek A. C., de Jong T., 1991, A&AS, 90, 55

Windhorst R. A., Miley G. K., Owen F. N., Kron R. G., Koo D. C., 1985, ApJ, 289, 494

Windhorst R. A., Fomalont E. B., Partridge R. B., Lowenthal J. D., 1993a, ApJ, 405, 498

Windhorst R. A., Fomalont E. B., Partridge R. B., Lowenthal J. D., 1993b, in the Milano International Symposium on "Observational Cosmology", Eds. G. Chincarini, A. Iovino, T. Maccacaro, & D. Maccagni, ASP Conf. Ser. Vol. 51 (Provo, UT: BookCrafters, Inc.), 534–540 "Limits to the 8.4 GHz Nano-Jansky Source Counts and Arcmin-Scale CBR Fluctuations"

Windhorst R. A., Fomalont E. B., Kellerman K. I., Partridge R. B., Richards E., Franklin B. E., Pascarelle S. M., Griffiths R. E., 1995, Nature, 375, 471

Windhorst R. A., 1999, in “The Most Distant Galaxies,” Eds. H. J. A. Röttgering, P. N. Best, M. D. Lehnert, Dordrecht: Kluwer (in press)

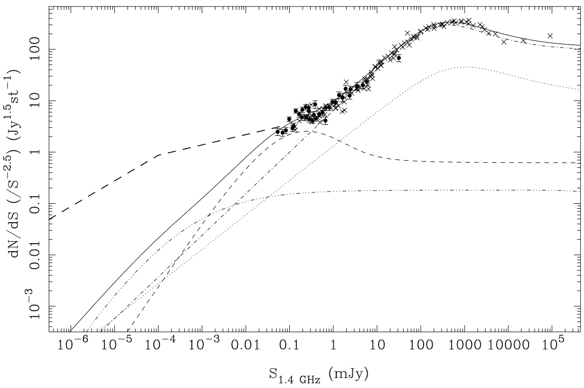

Fig. 1.— Models of the source counts showing relative contributions of different populations. Thin dashed line: IRAS-type population; Dotted line: AGN flat-spectrum population; Dot-dashed line: AGN steep-spectrum population; Dot-dash-dotted line: normal galaxy population; Solid line: sum of all populations. The symbols are existing observational source counts (see text). The normal galaxy population shown here is the maximum possible contribution supplementary to the other models and consistent with the observations. The thick dashed line represents the upper limit to the source counts implied from CBR constraints. More details are given in the text.

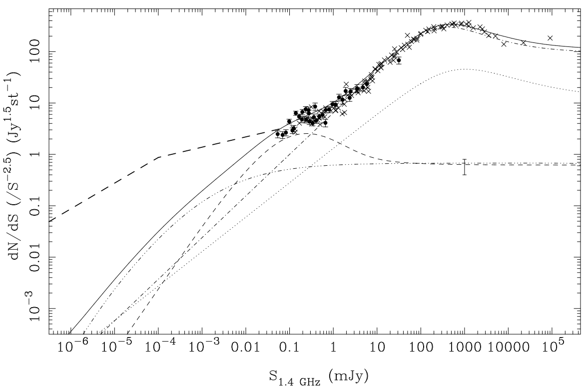

Fig. 2.— Models of the source counts. Here the evolution of the IRAS-type population is reduced from $Q = 3.3$ to $Q = 2.8$ and a greater contribution is made by the normal galaxies. The error bar shown on the IRAS-type source count indicates the range permitted by the uncertainty in the luminosity function normalisation. See text for details. Symbols and line styles are as for Figure 1. The upper limit to the source counts is again shown as the thick dashed line.

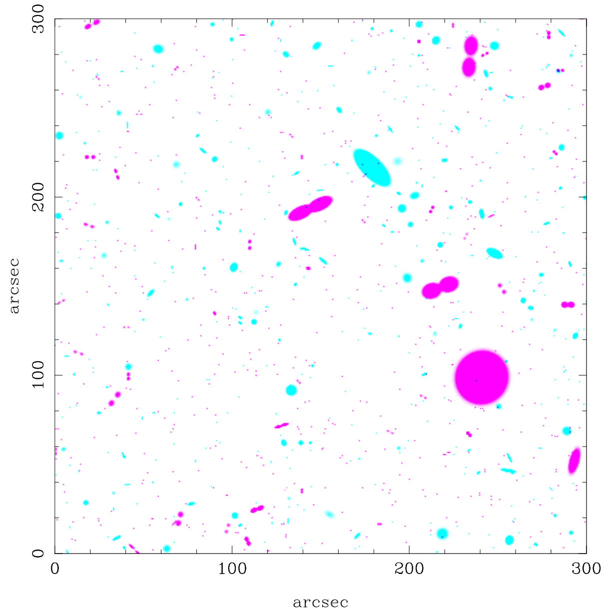

Fig. 3.— Simulated 1.4 GHz image. The image size is $5'$, with a flux density limit of $0.1\,\mu$Jy. There are 1008 objects in the simulation, divided into two categories: AGN (red, 574 objects) and starformers (blue, 434 objects).

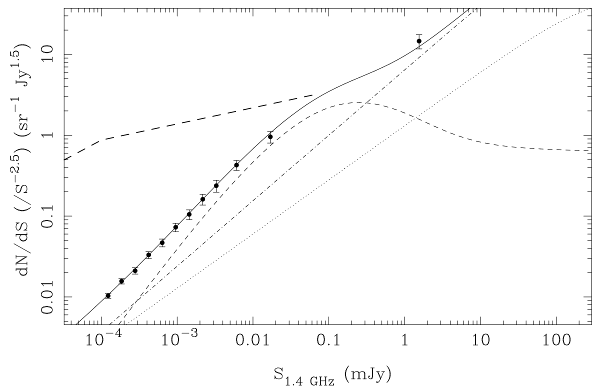

Fig. 4.— The source counts from the model luminosity functions (line styles as in Figure 1) used to produce the image in Figure 3, along with those calculated from a typical simulation (filled circles showing Poisson error bars), shown to confirm the self-consistency of the simulations. The upper limit to the source counts is again shown as the thick dashed line.

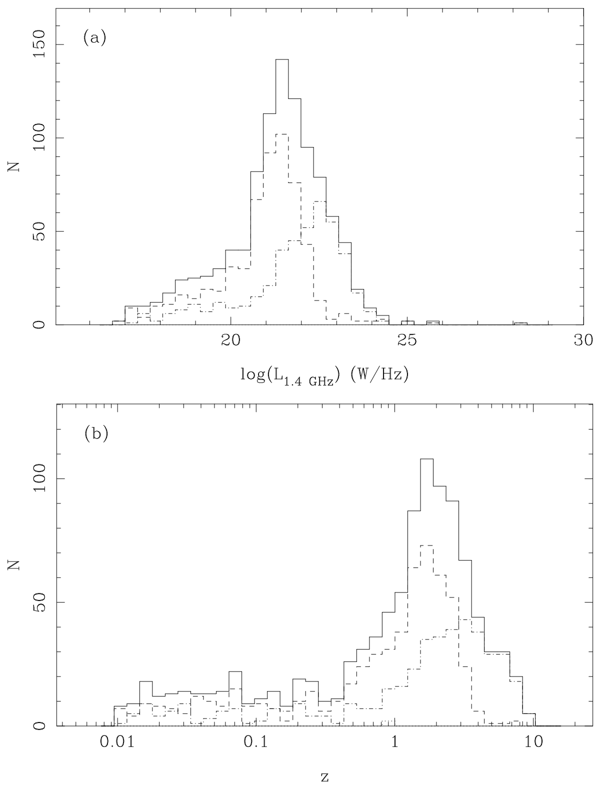

Fig. 5.— Distribution of (a) luminosities and (b) redshifts for the simulation in Figure 3. The line styles correspond to the different populations. Dashed: AGN; Dot-dashed: IRAS-type; Solid: the sum of all populations.

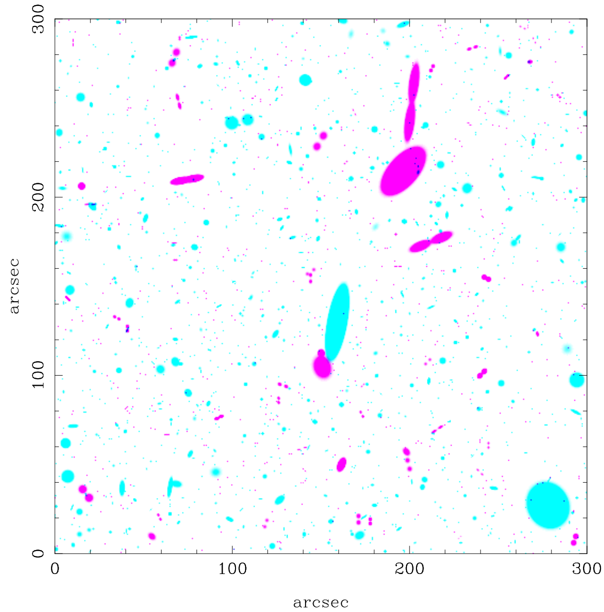

Fig. 6.— Simulated 1.4 GHz image. This simulation includes the population of normal galaxies in addition to the IRAS-types. The image is $5'$ on a side, with a flux density limit of $0.1\,\mu$Jy. There are 1941 objects in the simulation, 574 are AGN (red) and 1367 are starformers (blue).

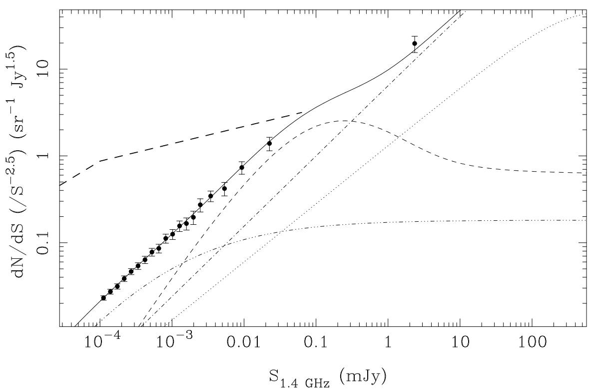

Fig. 7.— The source counts from the model luminosity functions, along with those calculated from a typical simulation, to confirm the self-consistency of the simulations (c.f. Figure 4). The new population of normal galaxies (dot-dash-dotted line) begins to make a noticeable contribution to the source counts below a few microjanskies. The upper limit to the source counts is again shown as the thick dashed line.

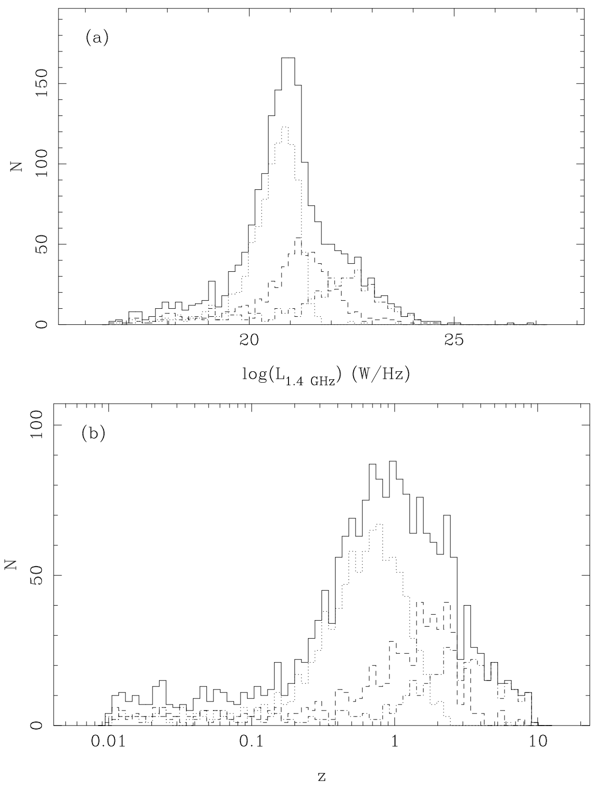

Fig. 8.— Distributions of (a) luminosity and (b) redshift for simulation in Figure 6. The line styles correspond to the different populations. Dashed: AGN; Dot-dashed: IRAS-type; Dotted: normal galaxies; Solid: the sum of all populations.